NAVAL POSTGRADUATE SCHOOL
Monterey, California

THESIS

ASSESSMENT OF DELFT3D MORPHODYNAMIC MODEL DURING DUCK94

by

Charlotte A. Welsch

September 2002

Thesis Advisor:	Edward B. Thornton
Thesis Co-Advisor:	Adrianus J.H.M. Reniers

Approved for public release; distribution is unlimited

THIS PAGE INTENTIONALLY LEFT BLANK

REPORT DOCUMENTATION PAGE			Form Approved OMB No. 0704-0188

Public reporting burden for this collection of information is estimated to average 1 hour per response, including the time for reviewing instruction, searching existing data sources, gathering and maintaining the data needed, and completing and reviewing the collection of information. Send comments regarding this burden estimate or any other aspect of this collection of information, including suggestions for reducing this burden, to Washington headquarters Services, Directorate for Information Operations and Reports, 1215 Jefferson Davis Highway, Suite 1204, Arlington, VA 22202-4302, and to the Office of Management and Budget, Paperwork Reduction Project (0704-0188) Washington DC 20503.

1. AGENCY USE ONLY *(Leave blank)*	**2. REPORT DATE** September 2002	**3. REPORT TYPE AND DATES COVERED** Master's Thesis

4. TITLE AND SUBTITLE: Assessment of Delft3d Morphodynamic Model During Duck94	**5. FUNDING NUMBERS**
6. AUTHOR(S) Welsch, Charlotte A.	
7. PERFORMING ORGANIZATION NAME(S) AND ADDRESS(ES) Naval Postgraduate School Monterey, CA 93943-5000	**8. PERFORMING ORGANIZATION REPORT NUMBER**
9. SPONSORING /MONITORING AGENCY NAME(S) AND ADDRESS(ES) N/A	**10. SPONSORING/MONITORING AGENCY REPORT NUMBER**

11. SUPPLEMENTARY NOTES The views expressed in this thesis are those of the author and do not reflect the official policy or position of the Department of Defense or the U.S. Government.

12a. DISTRIBUTION / AVAILABILITY STATEMENT Approved for public release; distribution is unlimited	**12b. DISTRIBUTION CODE**

13. ABSTRACT ***(maximum 200 words)***

Cross-shore wave transformation, nearshore currents, and morphology model predictions using Delft3D are compared with comprehensive observations acquired on a barred beach at Duck, North Carolina over a wide range of conditions. The Delft3D 2-DH model utilizes shallow water equations to phase resolve the mean and infragravity motions in combination with an advection diffusion equation for the sediment transport. Model coefficients and the effect of small changes in the wave incidence angle were examined for model sensitivity. The wave transformation model is dependent on the breaking parameter γ, which determines organized wave energy dissipation. γ was found to increase as a function of offshore H_{rms}. However, this is robust and a model skill of .89 was obtained using a constant γ = .425. The manning number *n* affects the current bed shear stress and determines the model current magnitude having an optimal value of *n* = 0.02. The model is not overly sensitive to the value of *n*. The asymmetry coefficient a_w determines the amount of onshore sediment movement. The rip channel created by mean currents on a short time scale is not affected by a_w whereas bar evolution requires more time to develop allowing a_w to affect morphology. A values of a_w = .25 gave the best results. Further research is needed to calibrate this parameter. Small changes in wave angle can cause significant errors for currents when complex bathymetry is present and the waves are near shore normal. Overall the model is robust with sensitivity to small changes in near normal wave angles.

13. SUBJECT TERMS Delft3D, Sediment Transport, Alongshore Current, Duck94, Wave Asymmetry, Nearshore Modeling, Wave Breaking Parameter, Infragravity Waves	**15. NUMBER OF PAGES** 55
	16. PRICE CODE

17. SECURITY CLASSIFICATION OF REPORT	**18. SECURITY CLASSIFICATION OF THIS PAGE**	**19. SECURITY CLASSIFICATION OF ABSTRACT**	**20. LIMITATION OF ABSTRACT**
Unclassified	Unclassified	Unclassified	UL

NSN 7540-01-280-5500 Standard Form 298 (Rev. 2-89)
Prescribed by ANSI Std. 239-18

THIS PAGE INTENTIONALLY LEFT BLANK

Approved for public release; distribution is unlimited

ASSESSMENT OF DELFT3D MORPHODYNAMIC MODEL DURING DUCK94

Charlotte A. Welsch
Lieutenant, United States Navy
B.S., United States Naval Academy, 1997

Submitted in partial fulfillment of the
requirements for the degree of

MASTER OF SCIENCE IN OCEANOGRAPHY

from the

NAVAL POSTGRADUATE SCHOOL
September 2002

Author: Charlotte A. Welsch

Approved by: Edward B. Thornton
Distinguished Professor of Oceanography
Thesis Advisor

Adrianus J.H.M. Reniers
NRC Fellow
Co-Advisor

Mary L. Batteen
Chairman, Department of Oceanography

THIS PAGE INTENTIONALLY LEFT BLANK

ABSTRACT

Cross-shore wave transformation, nearshore currents, and morphology model predictions using Delft3D are compared with comprehensive observations acquired on a barred beach at Duck, North Carolina over a wide range of conditions. The Delft3D 2-DH model utilizes shallow water equations to phase resolve the mean and infragravity motions in combination with an advection diffusion equation for the sediment transport. Model coefficients and the effect of small changes in the wave incidence angle were examined for model sensitivity. The wave transformation model is dependent on the breaking parameter g, which determines organized wave energy dissipation. g was found to increase as a function of offshore H_{rms}. However, this is robust and a model skill of .89 was obtained using a constant g = .425. The manning number n affects the current bed shear stress and determines the model current magnitude having an optimal value of n = 0.02. The model is not overly sensitive to the value of n. The asymmetry coefficient a_w determines the amount of onshore sediment movement. The rip channel created by mean currents on a short time scale is not affected by a_w whereas bar evolution requires more time to develop allowing a_w to affect morphology. A values of a_w = .25 gave the best results. Further research is needed to calibrate this parameter. Small changes in wave angle can cause significant errors for currents when complex bathymetry is present and the waves are near shore normal. Overall the model is robust with sensitivity to small changes in near normal wave angles over complex bathymetry.

THIS PAGE INTENTIONALLY LEFT BLANK

TABLE OF CONTENTS

THIS PAGE INTENTIONALLY LEFT BLANK

LIST OF FIGURES

ACKNOWLEDGMENTS

Dr. Thornton, I would like to express my earnest appreciation for all your direction, explanations, encouragement, editing ☺, patience, and most of all your time. Thank you for being my advisor and someone I deeply respect and admire.

Dr. Reniers, words cannot express the feelings of gratitude I have for your help over the past year. I have completely enjoyed working with you and have treasured your unfailing assistance for every angle of this thesis.

Finally, I would like to acknowledge my Lord and Savior for the hope that is in my heart and thank the Lord for growing me during this time in Monterey

THIS PAGE INTENTIONALLY LEFT BLANK

I. INTRODUCTION

A. MOTIVATION

Delft3D is being considered for transition as the new Navy surf model. Presently, the United States Navy uses the Navy Standard Surf Model, which is limited by simplified hydrodynamic equations (1-D) with the assumption of alongshore, uniform bathymetry. The 1-D assumption simplifies the equations, but neglects the effects of alongshore variations on near shore dynamics. 2-D modeling is required for increased accuracy of morphology predictions in the nearshore. For example, 2-D model computations can reproduce the development of alongshore bathymetry of shoals cut by rip-channels (Reniers et al., 2002). Many areas such as coastal management and engineering rely on predictions made by 2-D models and would benefit from their improvement. Naval applications include amphibious, special operations, mine, and mine counter measures and would benefit from the increased accuracy of the 2-D model.

The morphologic model that is examined is a research version of Delft3D. This 2-D model utilizes the nonlinear shallow water equations to phase resolve the mean and infragravity motions in combination with an advection diffusion equation for the sediment transport (Reniers et al., 2002). Once Deflt3D free parameters are calibrated and the model skill is established, the model can help improve the knowledge of near shore dynamics. Beach morphology is intricate and must be studied with realistic data to improve the understanding of the dynamics. Roelvink and Broker (1993) state the need for detailed comparisons and verifications of sediment transport models. Initially the standard Delft3D model results were compared with the L1P11D experiment conducted in the Delta flume in 1993. Both erosive and accretive 1-D experiments were accomplished (Arcilla et al., 1994). The model was calibrated with the flume measurements and the results showed that hydrodynamic predictions performed better than morphodynamic predictions. Arcillia et al. (1994) state the need for additional modeling efforts, particularly for sediment transport modeling. There has been a lack of model verification using field data. The research version of the hydrodynamic model has been qualitatively compared with more complex 2-D situations in the RDEX field experiment in Palm Beach Australia (Reniers et al., 2001) and the RIPEX field

experiment in Monterey Bay, USA (Reniers et al., 2002). The morphodynamic model is assessed here using field data acquired during the Duck94 experiment at Duck, North Carolina, where an amphibious vehicle recorded almost daily variability of near shore morphology.

B. OBJECTIVES

Beach morphology is important in determining near shore hydrodynamics. Waves and currents vary as the near shore topography varies. Bars affect cross-shore wave transformation and alongshore bathymetry variations produce alongshore pressure gradients forcing longshore and cross-shore currents. The objective of this thesis is to assess the Delft3D model morphodynamics by comparing model results with Duck'94 field data.

II. MODELING BAR MOTION

A. MECHANISMS OF BAR FORMATION

At least three processes have been identified that affect sandbar dynamics including wave asymmetry, undertow, and bound long waves. The break point hypothesis describes a mechanism of how sandbars are built. Outside the surf zone, there is an onshore movement of sediment by asymmetric wave motions. While inside the surf zone where waves break, the asymmetry decreases, and the set-up gradient drives an undertow, which transports the sand, stirred up by the wave motion, offshore. The wave asymmetry and undertow result in a convergence of sediment where the bar is located. In addition, wave group forced long waves outside the surf zone result in a seaward directed transport because of the concurrence of the bound-wave trough and the enhanced stirring during higher waves in a group (Roelvink and Stive, 1989).

Wave asymmetry, a mechanism associated with bar generation, moves sand onshore. Owing to the inherent nonlinearities of shallow water waves, the crests of harmonic components become phase-locked resulting in an asymmetry of wave velocities. This asymmetry of the waves results in stronger onshore flow under the crest than offshore flow under the trough. Sediment transport, s, is a function of the velocity associated with short waves $s \sim \left\langle u_s^{\,3} \right\rangle$ where u_s is the intrawave short wave velocity. The result is sediment is moved onshore owing to the asymmetry of the wave.

This onshore transport of sediments is countered by an offshore flux of sediment carried by the undertow. Waves produce an onshore mass flux due to wave drift and surf rollers confined primarily to the crest/trough region of the waves. This shore directed mass flux is compensated for by an offshore mean current below, the undertow. Wave breaking induced shear stresses are important in determining the vertical distribution of the mean velocity for undertow in the surf zone. The sediment stirred up by the wave motion is then carried off shore by this mean current.

In addition to wave asymmetry and undertow Roelvink and Stive (1989) include wave group-induced long wave flow in the bar generation. Sediment is stirred by short waves on a wave group time-scale and is then subsequently transported by the infragravity orbital motion $s \sim \left\langle u_s^2 u_l \right\rangle$ where u_l is the long wave velocity. Prior to wave breaking, bound long waves are forced by the groupiness of short waves in response to the changing short wave momentum. More sediment is put into suspension under the long wave trough stirred by the higher short waves than under the long wave crest where the short waves are lower. Since the velocity under the long wave trough is directed offshore, the resulting net sediment transport is offshore. Therefore, the short wave energy envelope and sediment transport are negatively correlated outside the surf zone (Figure 1).

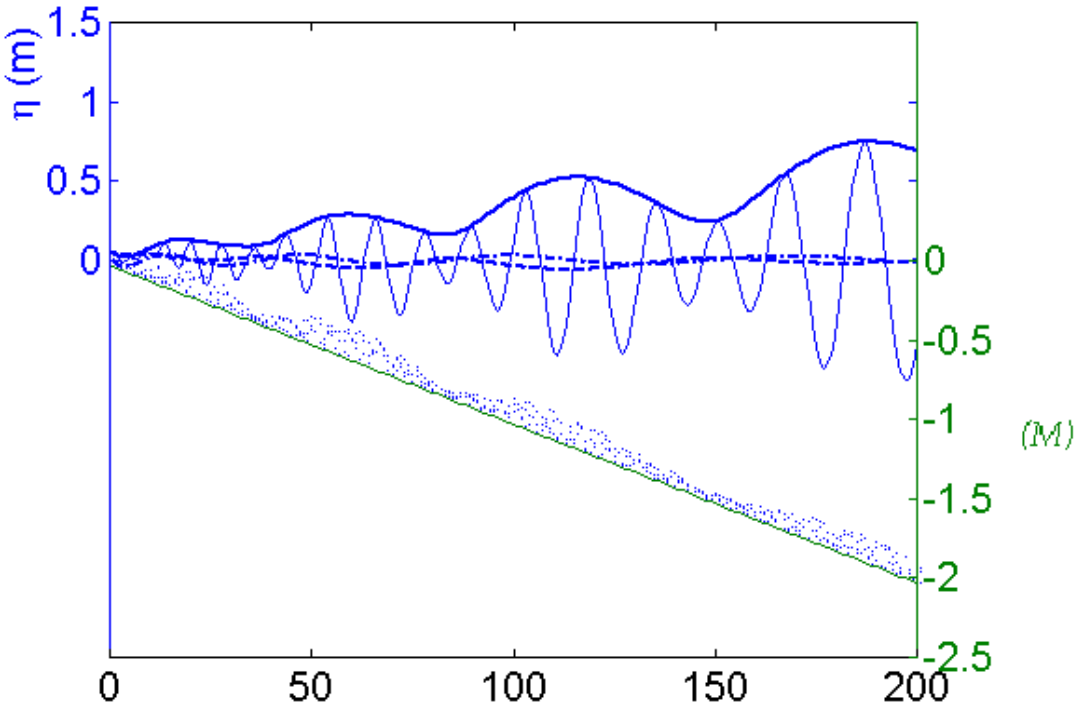

Figure 1. Depiction of wave groups normally incident on a beach with corresponding wave envelope (solid line), bound infragravity wave (dashed line) and free returning infragravity wave (dash-dotted line). Sediment is stirred under the short wave energy envelope.

Inside the surf zone, the short waves break decoupling the forced long waves, which then become free waves. Inside the surf zone, the height of the short waves and momentum flux generally decrease due to wave breaking. The decreasing momentum flux is balanced by a hydrostatic pressure gradient of the mean water level resulting in set up of the mean water level inside the surf zone. The breaking wave height is controlled by the total water depth, which is slowly (compared to the time scale of the short waves) modulated by the infragravity waves. Higher short waves (increased stirring of sediments) are now associated with the crest of the long wave (onshore velocity), whereas now the sediment transport and infragravity waves are positively correlated moving sediment onshore inside the surf zone.

How and to what degree infragravity waves affect bar generation is still in question. Thornton et al. (1996) and Gallagher et al. (1998) examined the beach at Duck, North Carolina for a variety of conditions and found that transport due to infragravity waves is generally subordinate in importance to asymmetry and the mean flow of longshore currents undertow. The infragravity sediment transport is not consistently in one direction, but alters as the cross-correlation changes throughout the surf zone. Ruessink (1998) and Roelvink and Stive (1989) all reason bar generation is the result of the varying degree of influence of multiple flow systems related to wave asymmetry, undertow, and infragravity waves.

THIS PAGE INTENTIONALLY LEFT BLANK

III. DESCRIPTION OF MODEL

A. OVERVIEW

Delft3D is a depth integrated one-, two-, or three-dimensional comprehensive modeling system. The model simulates flow, wave, sediments, and morphological progression. Initially Delft3D was developed for modeling 3-D flow in estuaries. This study will utilize a research version of the two-dimensional hydrodynamic and morphodynamic model. The research version of Delft3D has modified wave driver and sediment transport modules (Figures 2 and 3).

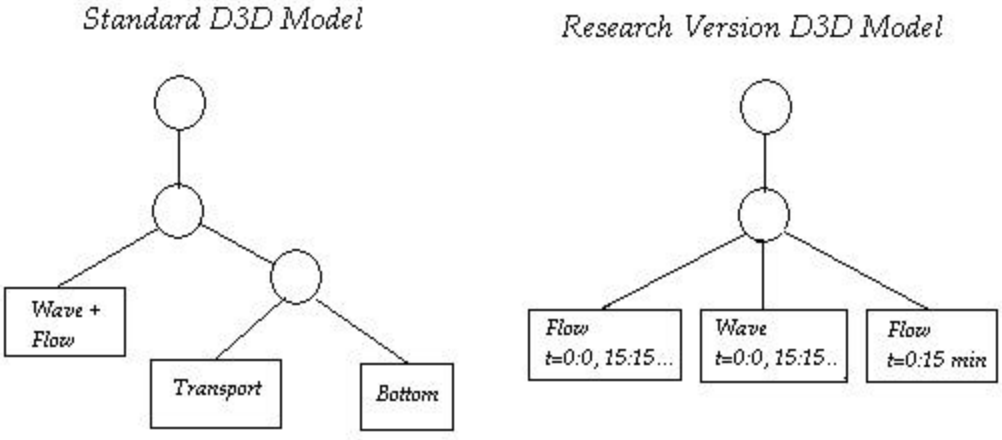

Figure 2. Delft3D Model Tree: The research model contains a restart file that takes data after 15 minutes and sends it to the initial flow to restart the computational loop.

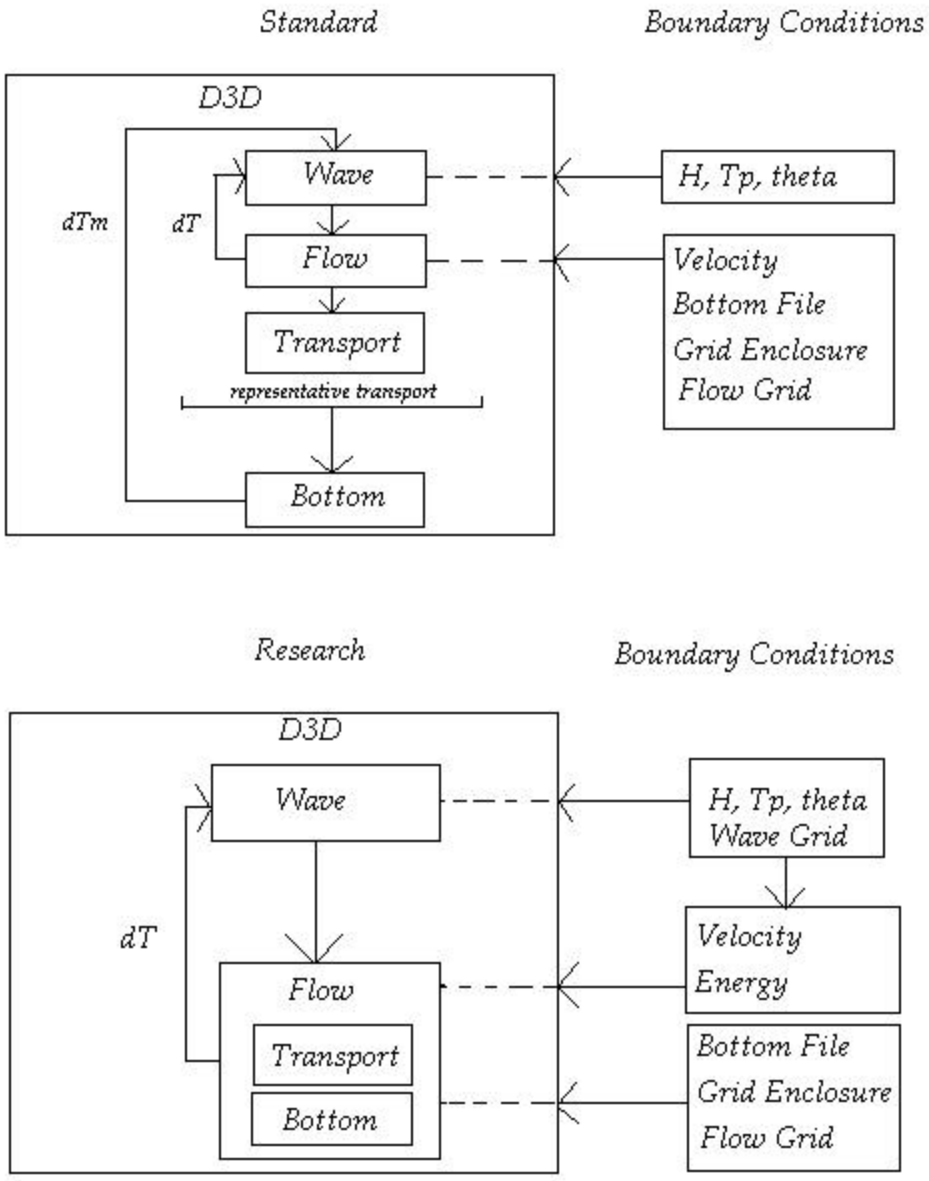

Figure 3. Delft3D Standard and research model: The research model does all of the above in one module instead of 4 separate modules. All information from one process is available to all other processes after each time step.

1. Wave Model

Delft3D-WAVE is a model used to simulate the propagation and transformation of wave energy from given initial environmental conditions of waves and wind over arbitrary bottom depths. In the standard version, the HISWA model (Holthuijsen et al.,

1989) is used to take into account wave generation due to wind, energy dissipation due to wave-bottom interactions, and non-linear wave-wave interactions. In the research version, the waves are phase-averaged over high frequency swell, but the infragravity band waves are phase resolved. HISWA solves for c_g and q using the initial conditions and bathymetry. The short wave energy, E_w, is solved through the energy flux balances given by:

$$\frac{\partial E_w}{\partial t} + \frac{\partial E_w c_g \cos(q)}{\partial x} + \frac{\partial E_w c_g \cos(q)}{\partial y} = -D_w \tag{1}$$

where c_g is the group velocity, q is the incidence angle with respect to the x-axis, x is the distance in the cross-shore, y is the distance in the alongshore, and D_w is the wave energy dissipation. The dissipation, or decrease in organized wave energy, is used as the input for the roller energy flux model described below. Dissipation is modeled as $D_w = P_b D_b$ where P_b is the probability that a wave is breaking and D_b is the dissipation rate in a breaking wave (Roelvink 1993). Both P_b and D_b vary on the time-scale of the wave groups. In the research model, the energy term of grouped short waves is used to calculate the forcing of the infragravity wave. The probability that a wave is breaking is a function of the energy of the waves, E, and total water depth, h, defined as:

$$P_b(E,h) = 1 - \exp\left[-\left(\frac{E}{g^2 E_{ref}}\right)^{n/2}\right] \tag{2}$$

where $E_{ref} = \frac{1}{8}\rho g h^2$, ρ is the mass density of water, g is gravitational acceleration, and g is the wave breaking parameter, and n is a dissipation parameter corresponding to the randomness of the incident waves. The dissipation of a breaking wave is analogous to the dissipation of a bore (Battjes and Janssen 1978), $D_b = 2\alpha f_p E$, which is a function of the energy of breaking waves, the frequency, f_p, at the peak of the wave spectrum and a calibration coefficient, α, set equal to one. The total dissipation is found by multiplying P_b and D_b :

$$D_w = P_b D_b = \left[1 - \exp\left[-\left(\frac{E}{g^2 E_{ref}}\right)^{\frac{n}{2}}\right]\right] 2af_p E \tag{3}$$

The breaking waves are assumed to form propagating bores, or rollers, inside the surf zone. Time is needed to convert organized kinetic energy and potential energy into small-scale, dissipative turbulent motion that results in a temporal lag between initiation of breaking and eventual dissipation of wave energy. The breaking wave energy is used as the input, or source, to the roller energy flux equation,

$$\frac{\partial E_r}{\partial t} + \frac{\partial 2E_r c_p \cos(q)}{\partial x} + \frac{\partial 2E_r c_p \cos(q)}{\partial y} = -D_r + D_w \tag{4}$$

where E_r is the kinetic energy of the roller, c_p is the phase speed, and D_r is the turbulent energy dissipation in the roller given by Nairn et al. (1990),

$$D_r = \frac{2g \sin(b) E_r}{c_p} \tag{5}$$

where b is the angle of the roller face and is set equal to 0.1. Therefore, the only free parameter to be determined in the Delft3D-Wave driver is the wave breaking parameter (g).

2. Flow Model

Delft3D-FLOW calculates non-steady flow forced by waves, tide, and wind. This module provides the hydrodynamic basis for morphological computations. The infragravity waves are solved in the time domain using the nonlinear shallow water equations to phase resolve bound and free, trapped (edge waves) and leaky infragravity waves. The flow module solves an unsteady shallow water equation for an incompressible fluid to obtain a two-dimensional (depth averaged) simulation. The

velocity field is composed of the Eularian velocity, u^E, and includes the short wave drift velocity (Stokes 1847),

$$u = u^E + u^S \cos(q) \tag{6}$$

The Stokes drift, $u^s = \frac{M_x}{rh}$, (Phillips, 1977) must be subtracted from the computed velocities, u and v, to solve for transport velocities. M_x includes the contribution of the roller in the mass flux.

$$M_x = \frac{(E_r + 2E_r)\cos(q)}{c} \tag{7}$$

In this approach, the vertical momentum equation is reduced to the hydrostatic approximation, i.e. vertical accelerations are assumed to be small compared to the gravitational acceleration and thus neglected. The depth-averaged continuity equation is given by:

$$\frac{\partial h}{\partial t} + \frac{\partial (hu)}{\partial x} + \frac{\partial (hv)}{\partial y} = 0 \tag{8}$$

where u and v are the wave group velocities in the x and y directions. Also $h = d + h$, where h is the total water depth, h is the mean water level, and d is still water level. The momentum equations in the x- and y- direction are:

$$\frac{\partial u}{\partial t} + u\frac{\partial u}{\partial x} + v\frac{\partial u}{\partial y} + g\frac{\partial h}{\partial x} + \frac{t_x}{rh} - \frac{F_x}{rh} - n\left(\frac{\partial^2 u}{\partial x^2} + \frac{\partial^2 u}{\partial y^2}\right) = 0 \tag{9}$$

$$\frac{\partial v}{\partial t} + u\frac{\partial v}{\partial x} + v\frac{\partial v}{\partial y} + g\frac{\partial h}{\partial y} + \frac{t_y}{rh} - \frac{F_y}{rh} - n\left(\frac{\partial^2 v}{\partial x^2} + \frac{\partial^2 v}{\partial y^2}\right) = 0 \tag{10}$$

where $t_{x,y}$ are the x and y component of the bed shear stress, which varies at the time

scale of the wave groups, and n is the turbulent eddy viscosity. *Fx* and *Fy* are the *x* and *y* components of the wave-induced forces:

$$Fx = \left(\frac{\partial S_{xx}}{\partial x} + \frac{\partial S_{yx}}{\partial y} \right) \qquad Fy = \left(\frac{\partial S_{yy}}{\partial y} + \frac{\partial S_{xy}}{\partial x} \right) \tag{11}$$

where S_{ij} are the components of wave momentum, or radiation stresses. The terms of the momentum equations in the *x*- and *y*- direction (going from left to right) are local change in velocity, advection terms, pressure gradient, bottom stress, external forces (wind and waves), and turbulent mixing.

Waves and currents are two important hydrodynamic factors that dominate the coastal zone. The model takes into account the generation of currents by waves, such as undertow and longshore currents. Using time dependent depth averaged shallow water equations allows shear instabilities of mean sheared currents to develop.

The bed shear stress of currents is enhanced by waves in the model. Bed shear stress is described through a non-linear wave-current interaction within the bottom boundary layer, where turbulent shear stress is proportional to the velocity squared, $t \propto u^2$ (Soulsby et al. 1993). Bed shear stresses for currents and waves alone are separately calculated and then combined. The current bed stress is found using the Manning formulation: $t_c = r C_z \left| U^2 \right|$ where $|U|$ is the magnitude of the depth averaged horizontal velocity, the drag coefficient $C_z = \frac{g n^2}{\sqrt[3]{h}}$, and *n* is the Manning coefficient. The magnitude of the bed stress due to waves is computed by: $t_w = \frac{1}{2} r f_w \hat{U}_{orb}{}^2$ where $\hat{U}_{orb}$ is the amplitude of the near-bottom wave orbital velocity and f_w is the wave friction factor. The Soulsby parameterization of the Fredsoe (1984) model combines wave-current flow and time-mean bed shear stress, $t_m = y(t_c + t_w)$, where $y = x\left[1 + bx^p (1-x)^q\right]$ and $x = \frac{t_c}{(t_c + t_w)}$ and *b*, *p*, and *q* are fitting coefficients.

3. Sediment Transport Model

The research model computes sediment transport on the same time scale as the flow. An advection/diffusion equation model is used to for sediment transport (Galapatti, 1983).

$$\frac{\partial}{\partial t} hC + \frac{\partial}{\partial x} hCu^E + \frac{\partial}{\partial y} hCv^E = \frac{hC_{eq} - hC}{T_s} \tag{12}$$

where C is the sediment concentration, w_s is sediment fall velocity, and T_s is the adaptation time for the diffusion of the sediment given by,

$$T_s = 0.05 \frac{h}{w_s} \tag{13}$$

The equilibrium sediment concentration is obtained by the Soulsby-van Rijn sediment transport formulation (Soulsby 1997).

$$C_{eq} = \frac{r\left(A_{sb+} A_{ss}\right)}{h} \left(\left(\left(\overline{u}^E + \overline{v}^E\right)^2 + \frac{.018 u_{rms}^2}{C_d} \right)^{\frac{1}{2}} - u_{cr} \right)^{2.4} \left(1 - 3.5m\right) \tag{14}$$

where A_{sb} and A_{ss} are the bed load coefficients which are a function of the sediment grain size, relative density of the sediment, and the local water depth (Soulsby 1997). Presently A_{sb} and A_{ss} do not include additional stirring of sediment by infragravity motions (van Rijn, 1993). The infragravity motions are assumed to be implicit in the near-bed orbital motion. To include infragravity velocities in the sediment stirring requires a recalibration of A_{sb} and A_{ss}. $C_d = \left[\frac{.40}{1 + \ln\left(\frac{z_o}{h}\right)} \right]$ where the drag coefficient, C_d, is due only to the mean current in which z_o is set to .006. m is the local bed-slope. u_{cr} is the critical threshold that the mean and orbital velocities must surpass to stir sediment. $\overline{u}^E$ and $\overline{v}^E$ are the mean (averaged over many wave groups) Eulerian

velocities that stir the sediment, and u_{rms} is the combined wave breaking induced turbulence motion and near bed short wave velocity,

$$u_{rms} = \sqrt{u_{rms,s}^2 + 0.5k_b} \tag{15}$$

The near bed, wave breaking induced turbulence, k_b, is given by (Roelvink and Stive 1989).

$$k_b = \frac{\left(\frac{D_r}{r}\right)^{\frac{2}{3}}}{\exp\left(\frac{h}{H_{rms,s}}\right) - 1} \tag{16}$$

where $H_{rms,\,hi}$ is the short wave, root mean square wave height.

The research model calculates asymmetry by applying stream function theory using the local wave height, depth, and period as input to the time-integrated contribution of the wave non-linearity. Due to the sediment transport associated with asymmetric short waves and the phase lags between sediment transport and wave group motions, transport has been averaged over the peak wave period, T_p, giving the wave asymmetry related parameterized velocity $\tilde{u}$,

$$\tilde{u} = a_w \frac{\int_0^{T_p} C'_{eq}(t) u'_b(t) dt}{\int_0^{T_p} C'_{eq}(t) dt} \tag{17}$$

where C'_{eq} is the equilibrium sediment concentration and u'_b is the instantaneous near bed velocity (prime denotes intrawave variables). The wave asymmetry calibration factor, a_w, is obtained by optimizing computed and observed measurements. The wave asymmetry related velocity $\tilde{u}$ is added to u^E, the instantaneous Eulerian velocity. Bottom changes are obtained from continuity.

$$\frac{\partial z_b}{\partial t} = \frac{1}{r_s n_p} \frac{hC_{eq} - hC}{T_s} T_{morf} \tag{18}$$

where r_s is the sediment density, n_p is the porosity, and T_{morph} is a morphological time step.

THIS PAGE INTENTIONALLY LEFT BLANK

IV. DUCK94 EXPERIMENT

The data used for this study were acquired during the Duck94 experiment from September 1 until October 31, 1994 at the U. S. Army Corps of Engineers Field Research Facility (FRF) on a barrier island in the Atlantic Ocean. Two bars having a well-developed inner bar during this time period characterize the site. Waves and currents were measured with a cross-shore array of 15 bottom mounted bi-directional electromagnetic current meters and pressure sensors extending from near the shoreline to 4.5 meters depth (Figure 4).

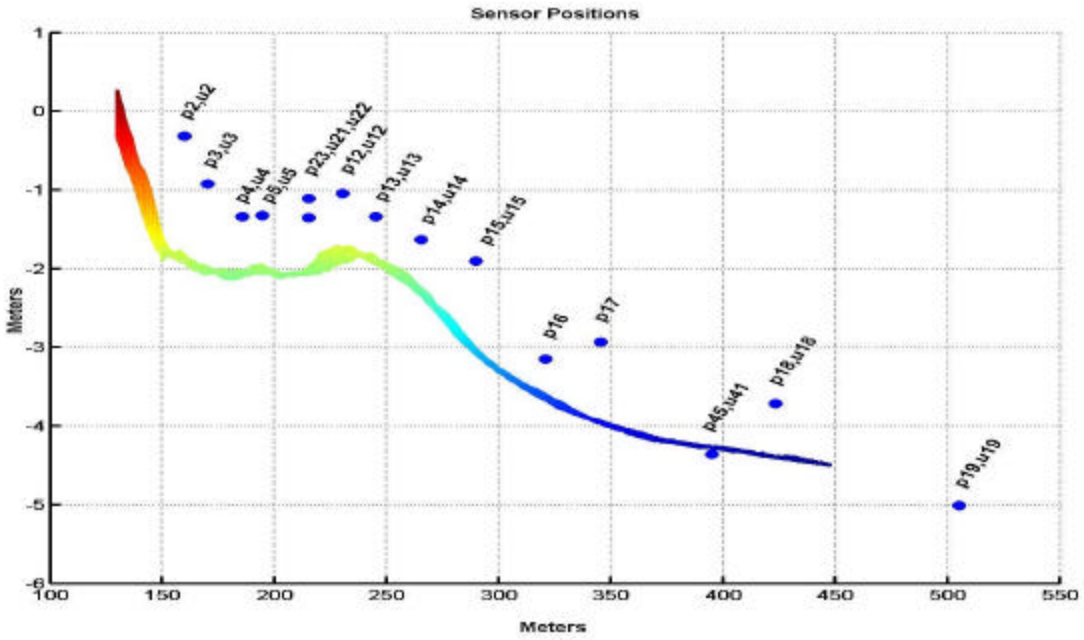

Figure 4. Sensor positions and bottom profile (relative to mean sea level). Location and elevation of numbered pressure and current sensors indicated by circles.

Offshore directional wave spectra, giving wave height, direction, period, and water depth, were measured using a linear array of 9 bottom mounted pressure sensors in 8m depth about 900m offshore. Data were sampled at 2 Hz. Bathymetric surveys were conducted regularly throughout the experiment by measuring the elevation and position using an amphibious vehicle (CRAB). The area surveyed, referred to as the minigrid, was 550m alongshore by 420m offshore composed of 18 cross-shore profile lines that where 25

meters apart near the instruments and 50 meters apart elsewhere. Details of the model calibration are described in the model calibration section that follows.

V. MODEL CALIBRATION

The accuracy of the modeling is determined by the model parameters chosen. The optimal breaking wave free parameter g is first determined for Deflt3D by examining a period of alongshore beach uniformity. A second time period of alongshore non-uniformity is chosen to study the 2-D affects on hydrodynamics and by model inputs, such as wave angle and wind data. The roller dissipation and bottom friction for both 1-D and 2-D are examined and set in accordance with the values found by Reniers et al. (in preparation 2002). The focus then turns to beach morphology by comparing the model and observed morphology with different asymmetry coefficients, a_w.

A. 1-D HYDRODYNAMIC CALIBRATION

The wave part of the hydrodynamic model was calibrated with data chosen from September 16th through the 28th (yeardays 259 – 271), when waves arrived at near normal incidence, wave refraction was small and did not effect dissipation. Directional wave data having three-hour averages were obtained from the FRF 8m linear array. H_{sig} ranged between 0.2 and 1.8 m, peak periods ranged between 3.2 and 15.6 s, and the wave angle ranged between 50° from the North and –38° from the South with a mean wave angle, $\bar{q}$, slightly from the South at -3.9 °degrees (Figure 5).

The only free parameter in the Delft3D-Wave driver is the wave breaking parameter g (eq.3), where nd=10, the manning coefficient n = 0.02, and a (eq.3) and b (eq.5) are set to 1 and .1 respectively. Adjusting b affects the dissipation of roller wave motion. By decreasing b, the model roller dissipation is decreased. The system for organized wave motion (wave height) is governed by g. If g is decreased, dissipation from wave breaking increases and H_{rms} approaches H_{max}.

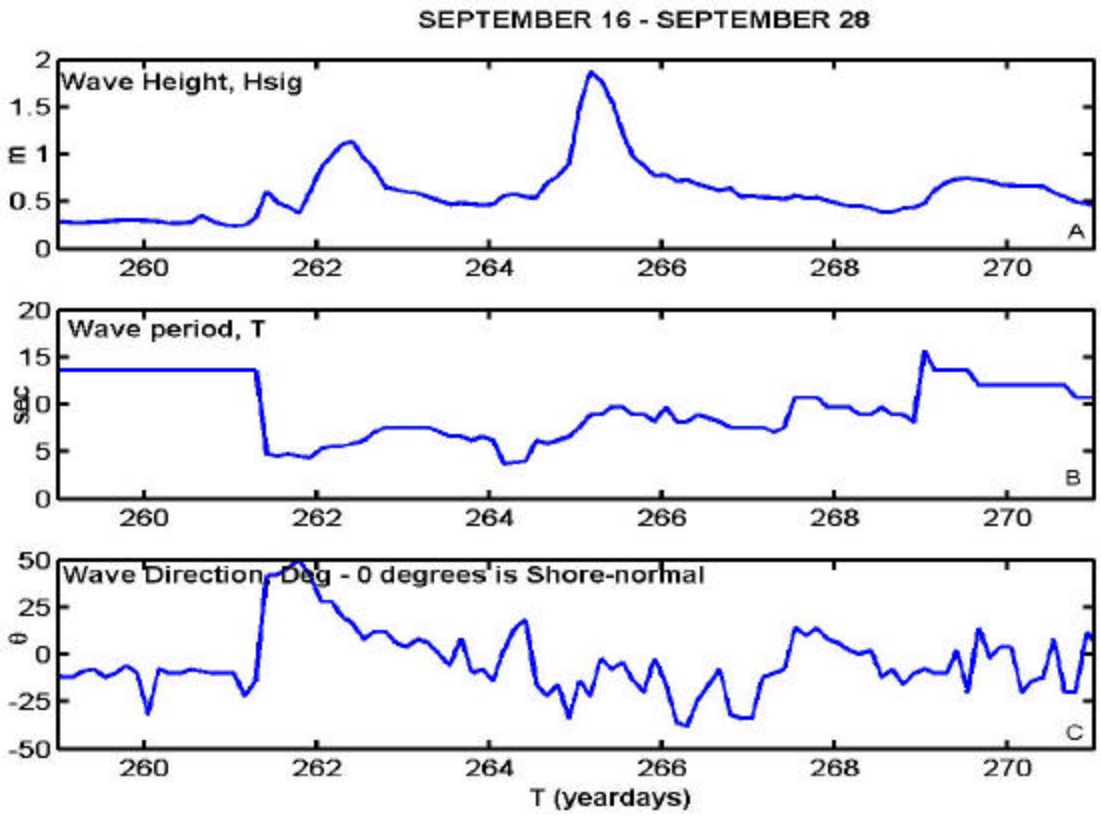

Figure 5. September 16-28 (yeardays 259-271) Wave Conditions:
Figure 6. (A) Significant wave height measured at 8m water depth. (B) Wave period at the peak of the spectrum. (C) Wave direction measured with waves propagating straight on shore having zero degrees, positive from the North and negative from the South.

Optimal g values were determined by comparing measured and computed wave heights for 15 model runs varying the wave breaking parameter (g) between .03 and .06. A linear regression was completed to minimize the error of the breaker parameter ? as a function of H_{rms} using model skill as a criterion. The skill is a scale where one is the highest value and indicates there is no difference between the model calculated data and the measured data.

$$skill = 1 - \sqrt{\frac{\frac{1}{N}\sum_{i=1}^{N}\left(V_{m,i} - V_{c,i}\right)^2}{\frac{1}{N}\sum_{i=1}^{N}\left(V_{m,i}\right)^2}} \tag{19}$$

where subscripts m and c denote measured and calculated data, and i is the instrument number.

The skill for g values from .3 to .6 were compared to H_{rms}, tide, and wave period. g was found to increase as a function of H_{rms} (Figure 6). The linear regression for the wave breaking parameter is $g = .074H_{rms} + .3180$. As H_{rms} increased, the optimal g for the model also increased. There was a broad area of high skill were waves varied between .6 and 1.2 meters. But as the waves increased in height the range of high skill decreased (Figure 6). Overall the model is not sensitive to reasonable variation of the wave breaking parameter g.

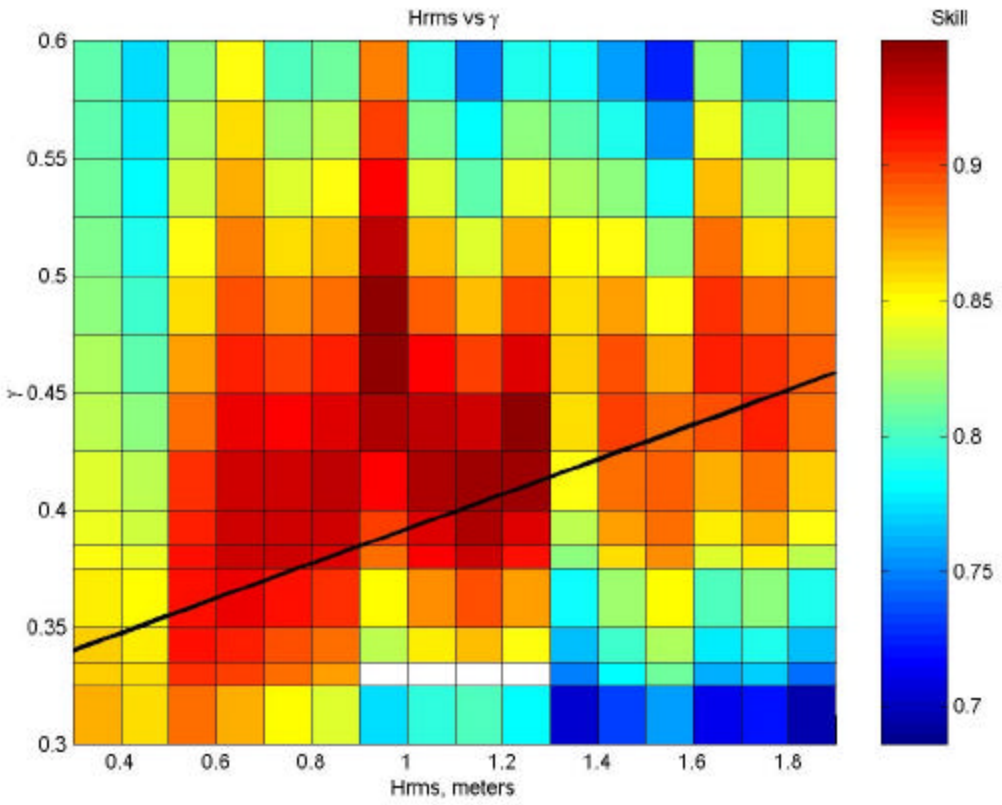

Figure 7. Skill plot (Hrms vs. g)

1-D hydrodynamics results found model and observed Hrms agree with an average skill of .89 for all 15 sensors for a g value of .425 during a thirteen-day period (Figure 7). A constant value of .425 was chosen for g throughout because the value

maintained the highest skill over the broadest range of wave height. The H_{rms} determined from pressure sensors from near shore (p5) to off shore (p19) are shown in Figure 7. The model was less accurate during the largest waves when the significant wave height reached about 1.8m. As the skill plot for g shows, the larger wave heights have a higher optimal g .

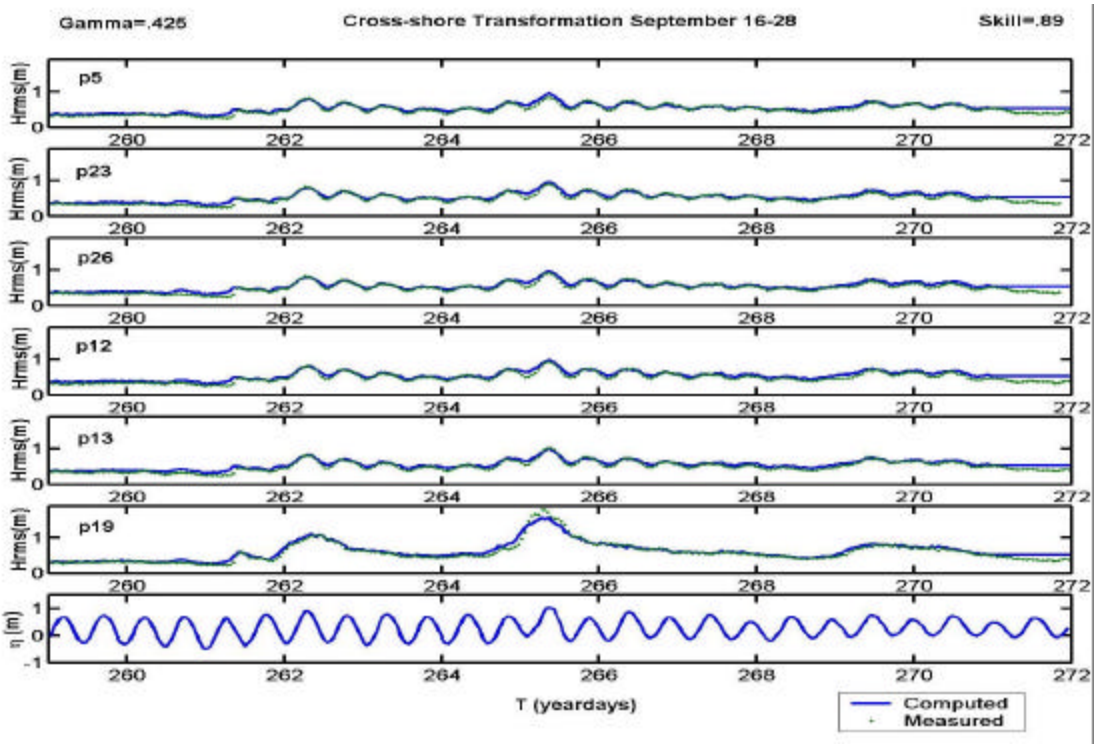

Figure 8. Cross-shore model and observed Hrms where modeled H_{rms} (line) and observed H_{rms} (dotted) are compared at different pressure sensors in the cross-shore using g = .425 and giving a mean skill of .89.

B. 2-D HYDRODYNAMIC CALIBRATION

The 2-D flow field is calibrated using data from October 10th through the 21st (yeardays 283 - 294) because this time period is strongly 2-D. The H_{sig} ranged between 0.4 and 2.1 m at the FRF linear array for three-hour averages. The mean period was approximated as the period of the first moment, T_{mo1}. T_{mo1} was computed by integrating the spectral density, *S*, and frequency, *f*, over frequency and direction.

$$\frac{1}{T_{mo1}} = \frac{\int\int_{f\ q} S(f,q)\, f\, df\, dq}{\int\int_{f\ q} S(f,q)\, df\, dq} \tag{20}$$

Mean periods ranged between 6 and 11.6 s with a mean of 8.5 s. The wave angle ranged from 21° from the North to –18.2° from the South having average mean wave angle, $\bar{q}$, slightly from the North at 1.2 °. An effective mean wave angle, $\bar{q}$, was computed that gives the same radiation stress calculated using linear theory as that determined from the full directional spectrum *E(f,q)* (see Thornton and Guza, 1986).

$$S_{xy} \approx \int\int_{f\,q} E(f,q)\frac{c_g}{c_p}\sin q\cos q\, df\, dq \;=\; \bar{E}\frac{\overline{c_g}}{\overline{c_p}}\sin\bar{q}\cos\bar{q} \tag{21}$$

Alongshore winds were acquired with an anemometer located 19.5 meters above mean sea level at the end of the FRF pier. The alongshore winds ranged from -5.16 to 14.15 m/s with a mean velocity from the North at 4.8 m/s over the time period specified (Figure 8).

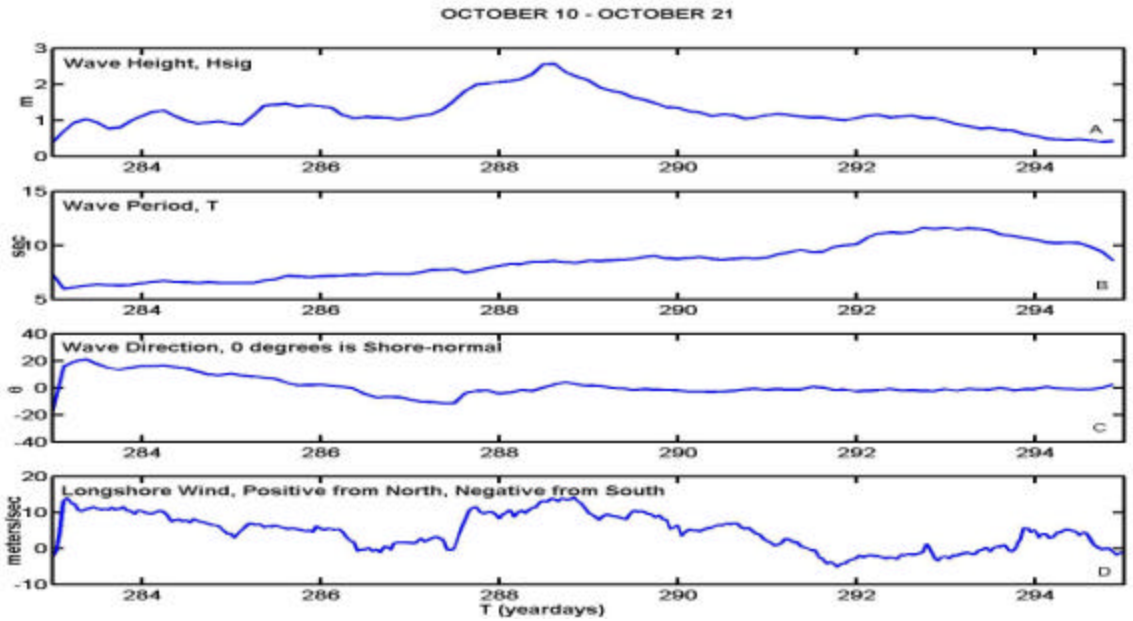

Figure 9. October 10-21 (yeardays 283-294) wave conditions. (A) Significant wave height measured at 8m water depth. (B) Wave period. (C) Wave direction measured with wave propagating straight on shore having zero degrees, positive from the North and Negative from the South. (D) Alongshore wind where positive is from the North and negative is from the South.

Daily minigrid bathymetry and monthly largegrid bathymetry were available and necessary to model the longshore current. The minigrid data from October 10, 11, 12, 14, 20, and 21 were superposed onto the September large-grid data to better resolve bathymetry at instrument locations. An extended flow field was needed to prevent boundary generated disturbances from affecting flow in the area of interest.

October 10-15 was a period of offshore bar motion during relatively high-energy conditions. The largest observed H_{rms} profile changes during the Duck94 experiment occurred between October 10th and 20th. Initially the beach was alongshore uniform as seen by the 10 October minigrid bathymetry. The 18 October survey clearly shows alongshore inhomogeneitics, which developed during the storm (Gallagher et al., 1998). Also a large rip channel developed in the minigrid during this time period (Figure 9).

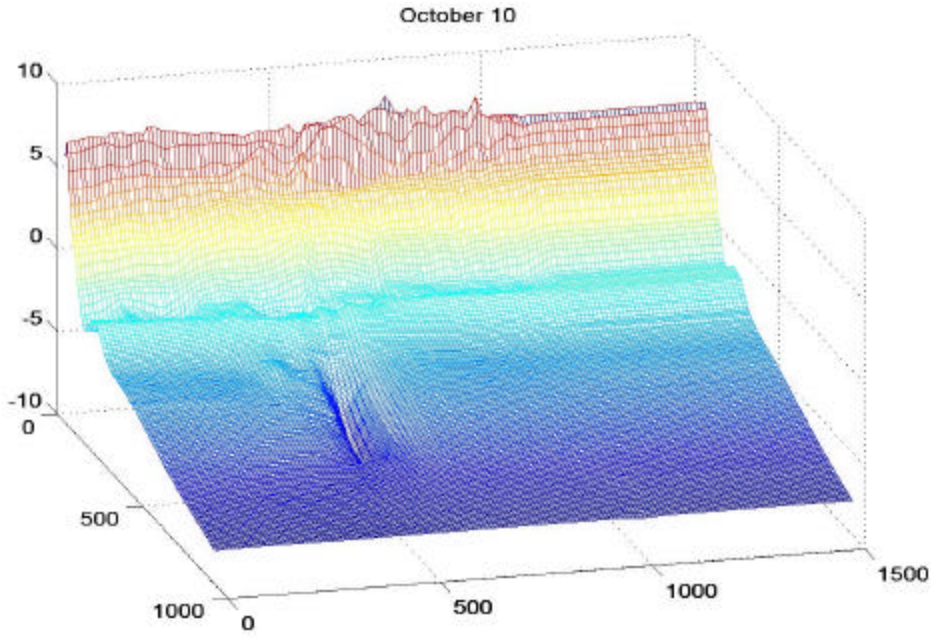

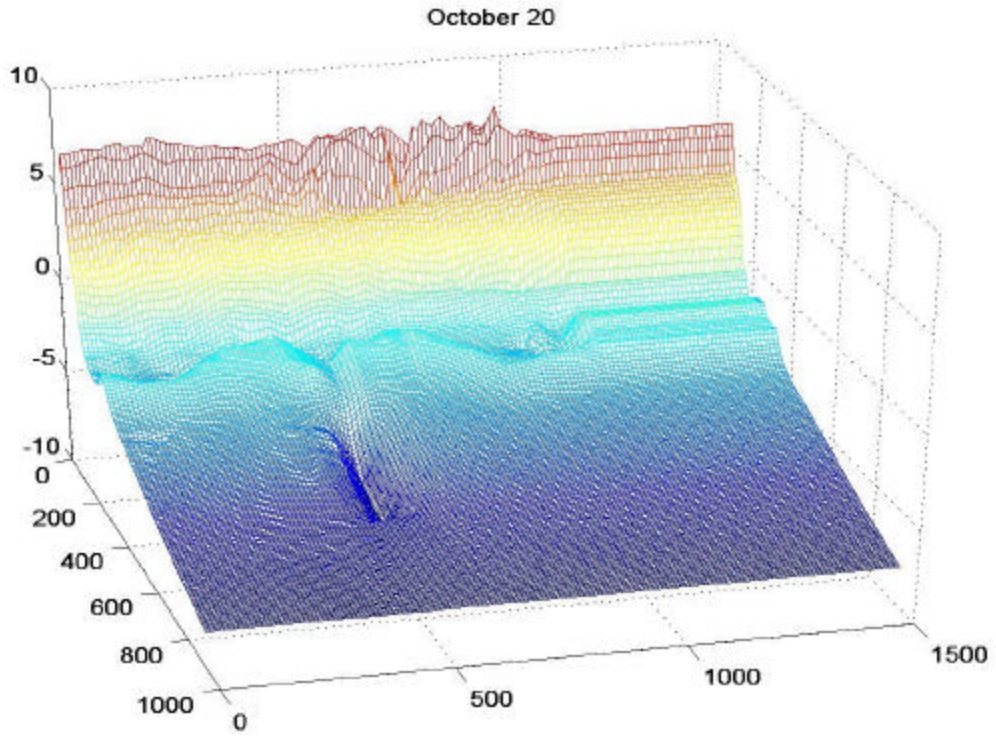

Figure 10. Grid for 10 and 20 October. The minigrid area shows the large rip channel (y=1000m), non-uniformity of the alongshore bathymetry, and the pier area (y=500m).

In the model, the largegrid was expanded to 2,500 meters alongshore maintaining a uniform ΔY and to 930 meters cross-shore with a systematically increasing ΔX from 5 meters starting at the shore to 30 meters offshore. The grid-size for the model was chosen considering accuracy and computational time. Originally the computational grid was with ΔX increasing offshore having 103 grid points and ΔY equal to 10 meters giving 179 grid points for a total of 18,437 computational grid points. By changing ΔX, while still increasing with distance offshore, to only 66 grid points and ΔY to 12.5 meters with 147 grid points, the total grid points were decreased to 9,702 decreasing computational time from 53 hours to 24 hours of computer time for 24 hours of real time. Comparing the skill for wave height and currents during October 10th, there was essentially no decrease in skill by changing the grid (Figure 10).

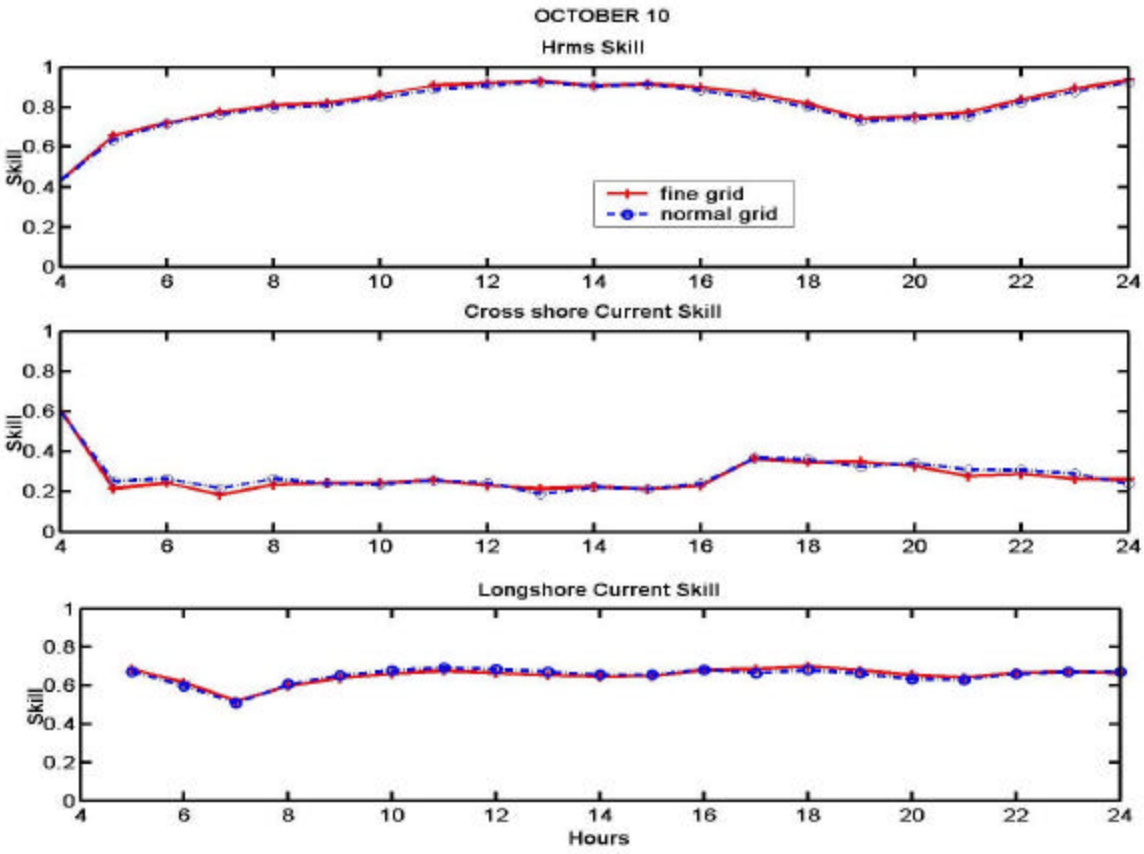

Figure 11. Skill comparison using different grids: $H_{rms,}$ u, and v model skill values for October 10th compared using a fine grid and a normal grid.

Delft3D uses an implicit finite difference numerical scheme (Stelling, 1984) to solve the momentum, continuity, and transport equations on a staggered grid. The Alternating Direction Implicit (ADI) technique is used and each time step is split into two stages. This scheme implicitly solves the water levels and velocities in the x-direction in the first half-step and the y-direction terms in the second half-step. Since the model is working at a wave group structure scale, the model allows for larger spatial scales with similar accuracy as smaller space scales.

The 2-D shallow water equations are time integrated using a Crank-Nicholson implicit finite difference approximation. The implicit numerical scheme makes the computations more stable, allowing for larger spatial steps while maintaining accuracy.

When calibrating the 2-D hydrodynamic part of Delft3D, the wind contribution was examined. The model improved when wind is included as a boundary condition as an example. The October 10th model run was completed with wind and without wind

input for comparison. The mean wind on October 10th was 9.8 m/s consistently coming from the North. The model run with wind data shows an increase in mean skill for the entire day (Figure 11). The mean skill for longshore current with no wind was .60, while the mean skill for longshore current with the wind was 0.65 showing an improvement of 8.3%.

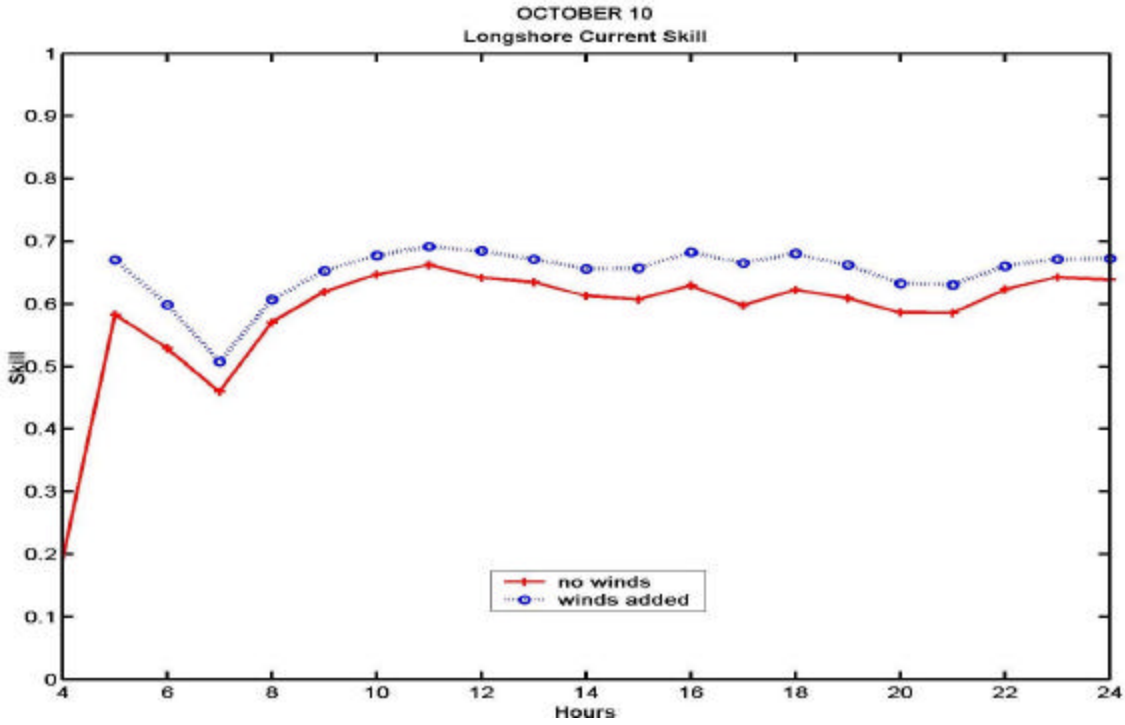

Figure 12. Longshore current skill compared with and without meteorology data.

Bottom roller dissipation and friction were examined and found consistent with Reniers et al. (in preparation 2002) using a roller dissipation coefficient, b = .1 and a Manning number of 0.02. If b is decreased, roller dissipation decreases and longshore current shifts toward the shore. The Manning number affects bed shear stress. If the Manning number is increased, friction increases, decreasing the model flow (Figure 12).

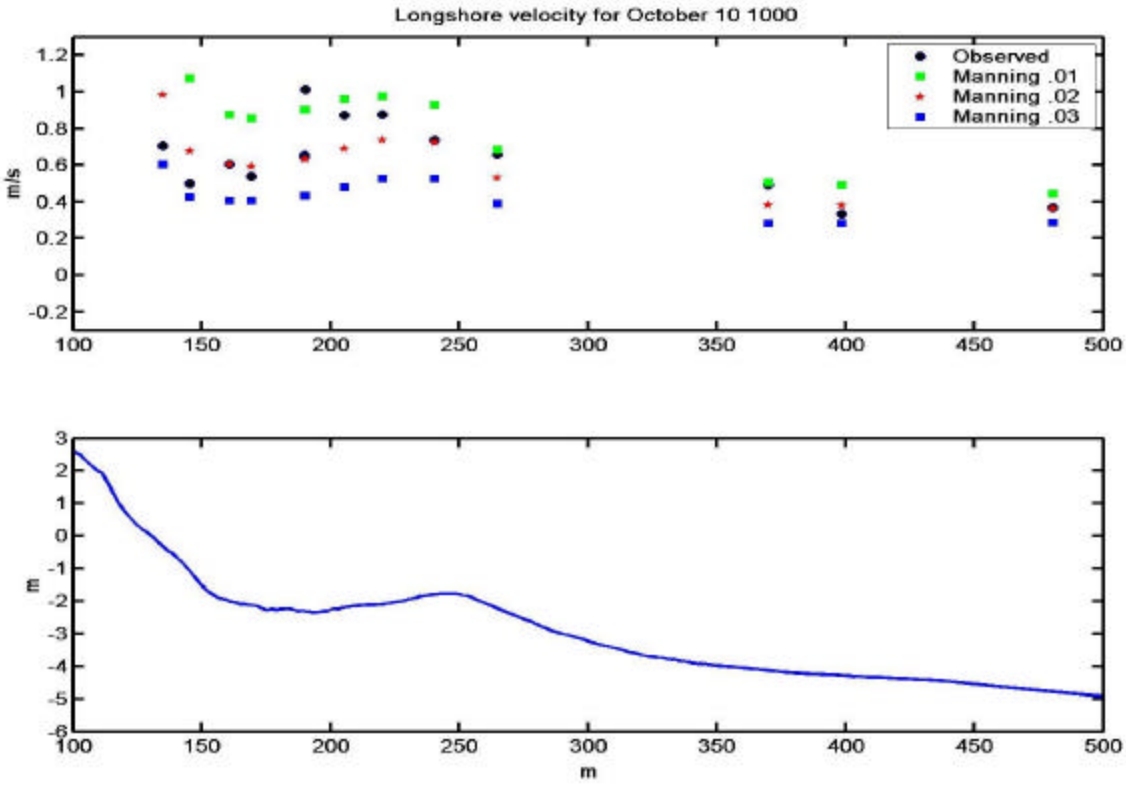

Figure 13. Longshore velocity and manning number changes.

Significant improvement in the modeled longshore current occurred when boundary conditions were modified. Initially, the North and South boundaries of the grid were reflective (v=0). When the longshore current approached the boundary, it was deflected offshore, but instead of fading away as depth increased it recirculated in the computational domain. The circulation caused the alongshore current furthest from the shore to be in the opposite direction as the current near the beach, which was in the same direction as the wind and wave angle. Therefore the reflective boundary conditions were replaced with water level boundary conditions that allow the flow to pass.

The overall longshore current velocity skill for the 10th through the 21st of October for all sensors was -0.2 (Figure 13). The beginning of the period showed

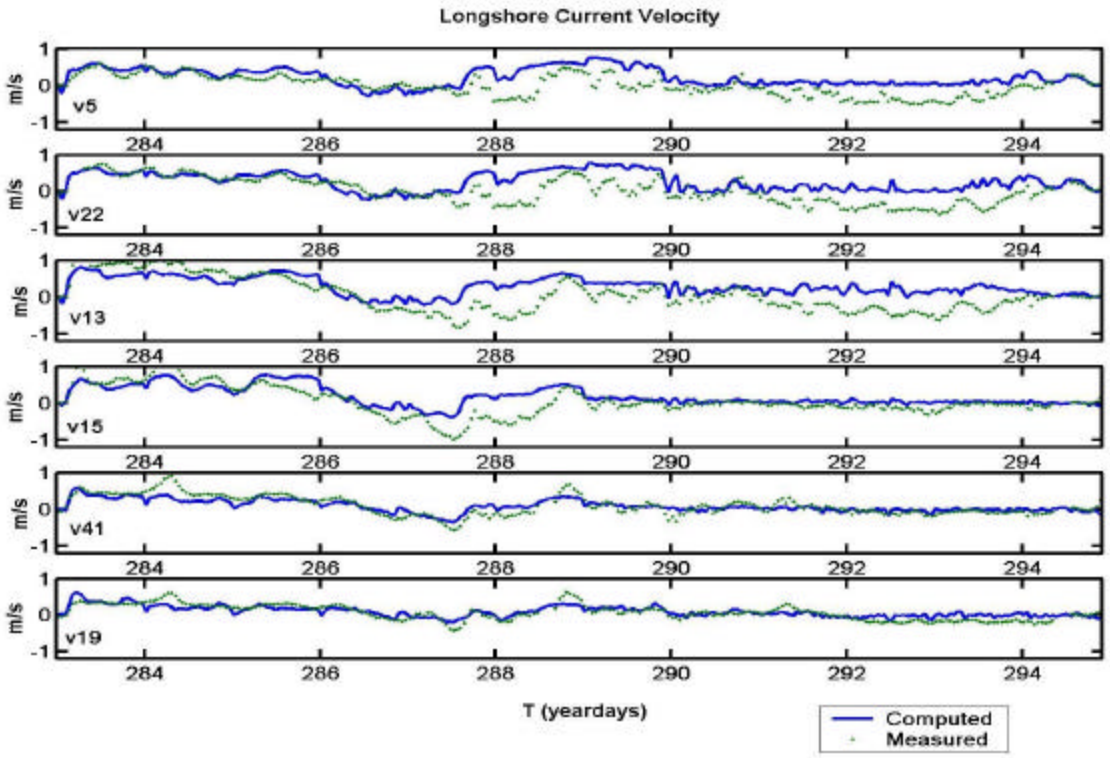

Figure 14. Longshore modeled and observed velocities where modeled longshore current (line) and observed longshore current (dotted) are compared at different velocity sensors in the cross-shore giving a mean skill of -0.2

reasonably high skill, falling off around October 14th (yearday 287) and then increasing again to October 21st (yearday 294). The bathymetry during this period changed significantly as the storm moved in, going from alongshore uniform to non-uniform with a large rip channel. The model performed better before the storm. Also due to the storm, the only bathymetry available was October 10, 11, 12, 14, 20, and 21. The model performed better when daily bathymetry was available (Figure 14). The longshore model velocity skill was affected more by the lack of bathymetry than the cross-shore velocity. The cross-shore skill improved when the rip current dominated the flow (yearday 288) due to the sensitivity of the skill factor when measurements are close to zero.

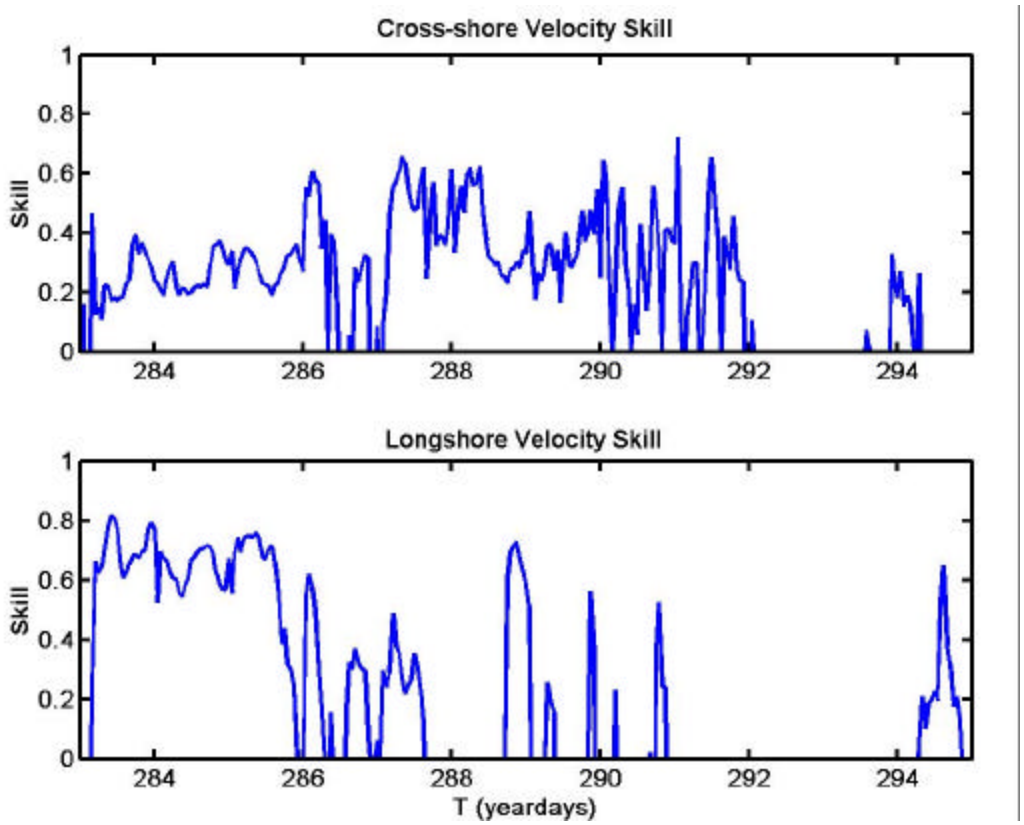

Figure 15. Cross-shore and longshore skill for 10-21 October with negative skill values are not shown.

Examining 19-20 October (yeardays 292-293) for sensors in the trough and on the bar (v5, v22, and v13) the modeled longshore velocities are greater than the near-zero observed longshore velocities. The wave angle during this time was near zero. When the bathymetry was alongshore uniform, small wave angle (slightly varying from shore normal) did not affect alongshore and cross-shore currents. However, small wave angles resulted in strong variability in alongshore currents during times of complex bathymetry, such as after the storm.

To show the sensitivity of the model, the 20th of October was examined because acceptable 2-D bathymetry information was available, the wave angle was shore normal, and the alongshore wind was minimal. Adjusting the wave angle by adding 2.5°, which is about the measurement error, the model was compared with a normal wave angle to determine how the computed results varied. As expected, H_{rms} did not change appreciably. On the other hand, the cross-shore current skill increased while the

longshore current skill decreased. The significant skill changes in opposite direction with such a small change in wave angle shows that currents and circulations in a rip channel are sensitive to small changes in wave conditions (Figure 15).

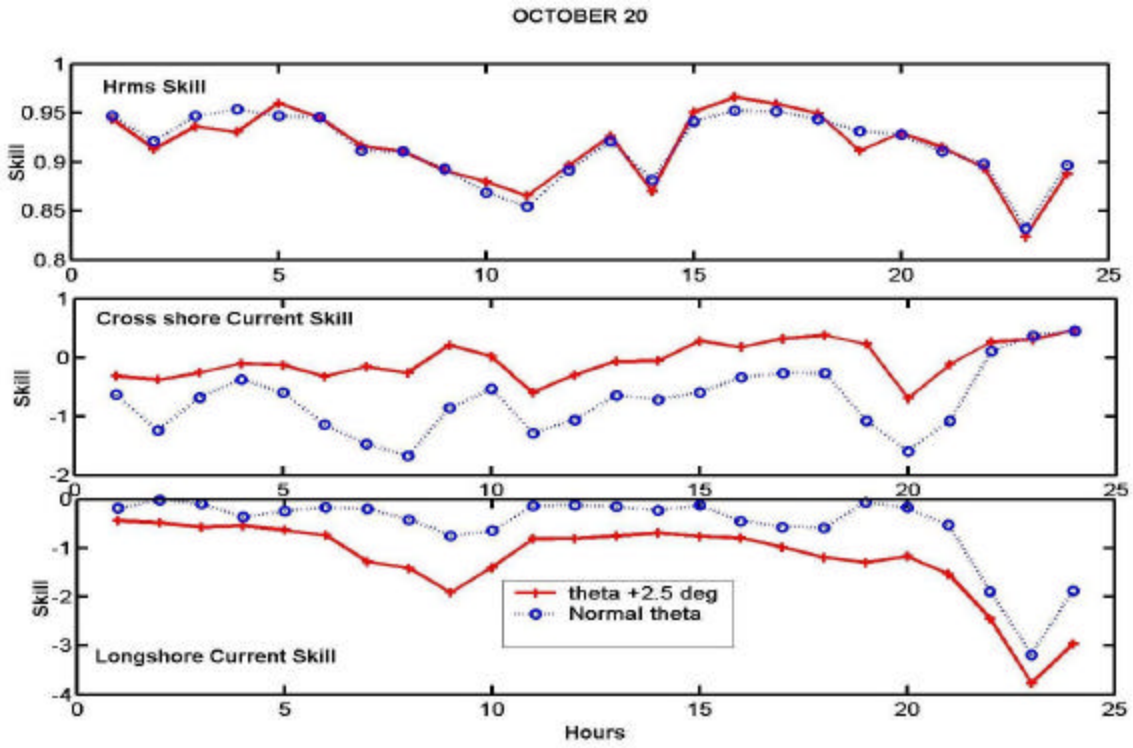

Figure 16. Skill comparison with 2.5° increased wave angle.

Looking closely at the end of the period, the skill improved from the 20th to the 21st of October (Figure 13), but at the same time, the bathymetry and alongshore wind were almost identical. The question still remains why there are these differences between the two days.

Another consideration for skill variations at this test location is the near proximity of the FRF 800m pier. The pier scour hole and pilings can influence the waves and currents and resulting morphology within the minigrid. The model does not consider the turbulent eddies from the pier or their effects on circulation.

THIS PAGE INTENTIONALLY LEFT BLANK

VI. 2-D MORPHOLOGY ASSESSMENT

The changes in morphology were examined for October 12th through the 16th by comparing with the minigrid bathymetry. Asymmetry as determined by the a_w value, is important in determining net sediment transport. a_w was examined by varying its values between .1 and .4. If a_w is decreased, onshore sediment transport is decreased, moving the bar offshore as sand erodes. The asymmetry is also a function of the wave period, where as the wave period increases, the asymmetry increases. The wave period increased throughout the period considered.

Examining a cross-shore profile transect at 180m North of the velocity sensors, increasing a_w significantly moved sediment onshore over the five day period (Figure 16).

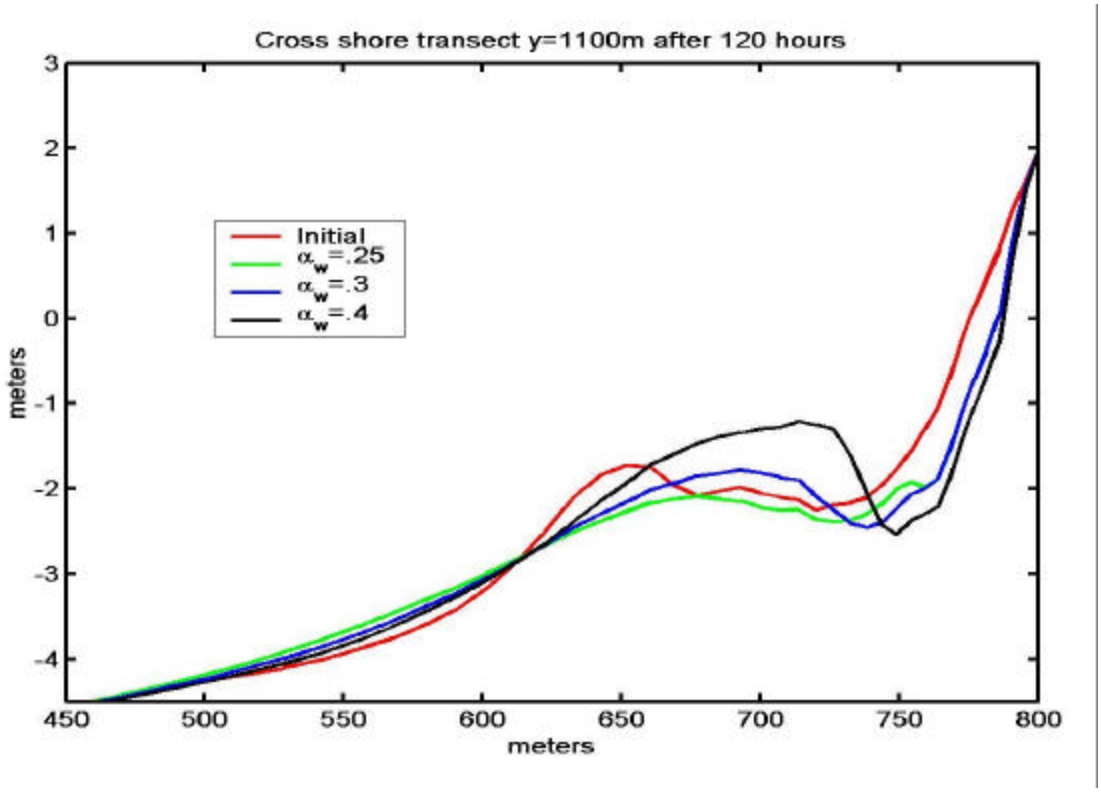

Figure 17. Cross-shore sediment transport while increasing a_w at y = 1100m.

However, in the rip channel where the velocity sensors are located, increasing a_w actually increased erosion and the sandbar moved further offshore and widened (Figure 17). The model deposited sand further offshore than in actuality. As asymmetry was

increased, more sand moved onshore, increasing the set-up and pressure gradients on either side of the channel. This increased forcing, increased the magnitude of the rip current. The model does not include wave-current interaction throughout the flow field, except for the bottom shear stress, so as the rip increased in strength there was no opposing force to slow it down. In reality incoming waves opposing the outgoing rip current cause the sand to be deposited closer to the shore than what the model predicts. The rip current channel was widened and deepened as a_w increased.

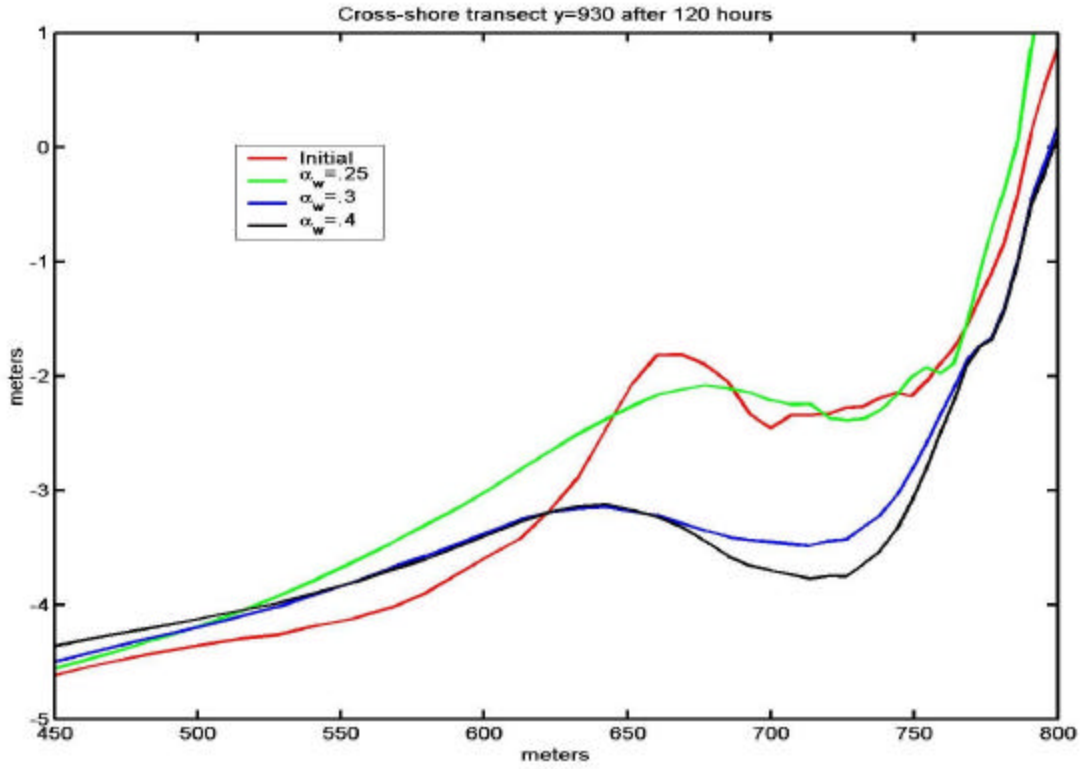

Figure 18. Cross-shore sediment transport while increasing a_w at y = 930m.

The modeled bathymetry for all a_w values eroded more alongshore near the beach than the observed bathymetry. This indicates that the alongshore current was stronger right near the shore than observed. By comparing the modeled and measured minigrids after five days, it appears a_w=.25 most closely simulates the 2-D changes in bathymetry (Figure 18).

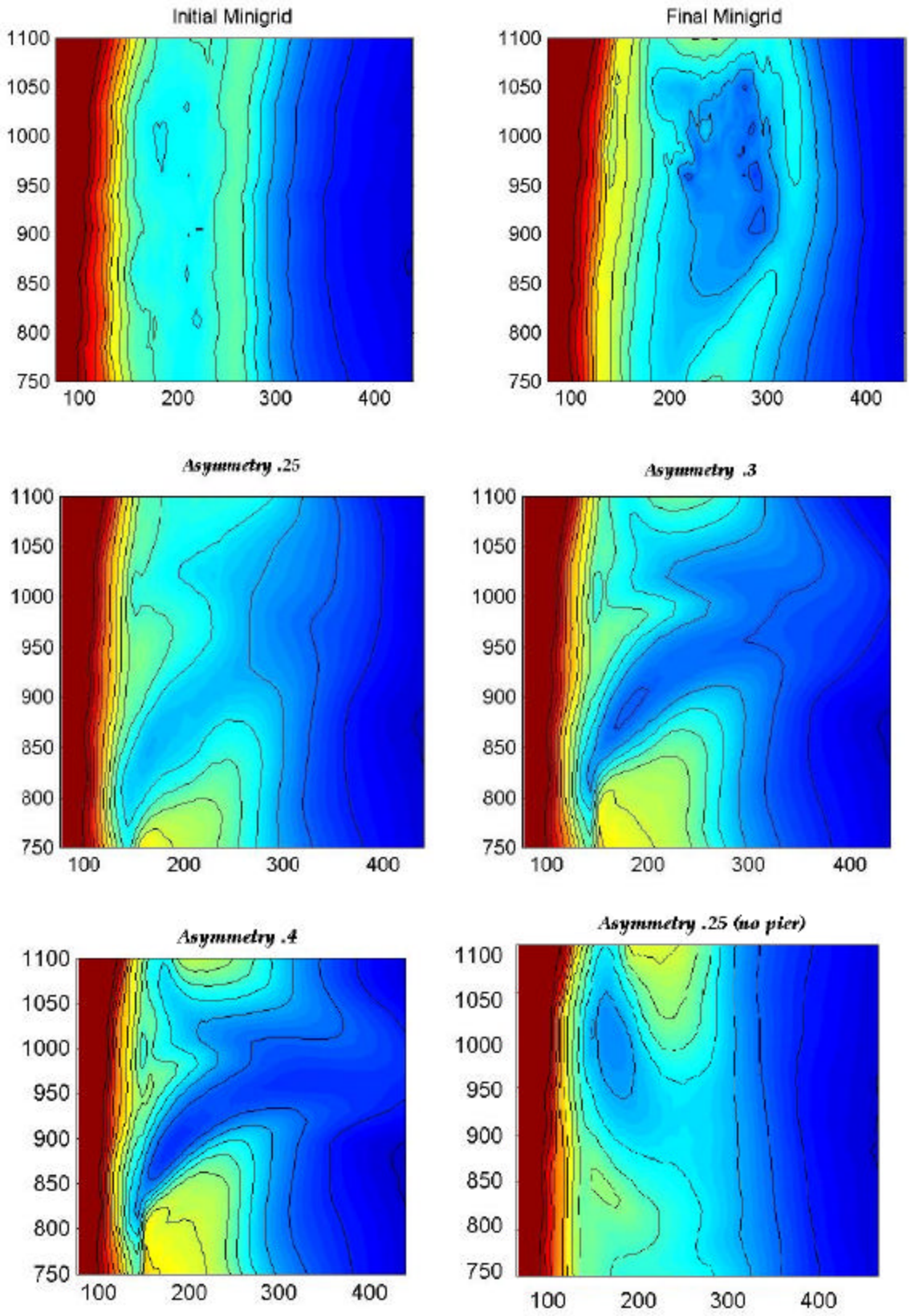

Figure 19. 2-d bathymetry showing rip channel.

The effects of the scour hole created by the FRF pier was examined next. A smoothed bathymetry was generated removing the pier scour hole to examine the circulation and morphology. It appears that the model leaves a large deposit of sediment at the Southern boundary of the minigrid when the pier is included. Also the rip channel has an orientation from the Southwest to the Northeast with the pier scour hole included in the model. Removing the effects of the pier, the orientation of the channel changes to the Northwest to the Southeast with a larger sediment deposit on the Northern boundary of the minigrid. From this it is clear the pier plays a significant role in the sediment dynamics in the area.

VII. CONCLUSIONS

Nearshore morphology and currents were measured nearly continuously for two months near Duck, North Carolina where September 16-28 and October 10-21 were two time periods identified to model. Wave height time series outside the surf zone show considerable variability in wave height associated with wave generation by local winds and distant storms. Strong winds from Nor'esters build waves increasing the radiation stresses and turbulent stirring of sediment. Due to near shore circulations, a rip channel developed and deepened due to the increased offshore forcing. Nearshore modeled H_{rms}, currents, and morphology were compared to data by the computed Delft3D 2-DH model utilizing shallow water equations to phase resolve the mean infragravity motions in combination with an advection diffusion equation for the sediment transport.

Energy dissipation due to wave breaking is extremely complex. The wave breaking parameter, g, utilized by Roelvink (1993), is critical in the decay of wave groups. Gamma is found to be a function of wave height having a concentration of high skill around gamma=.425 for a broad range of wave heights. Interestingly, Roelvink (1993) found a higher optimal value of gamma using lab data of .57. From the verification presented (Figure 6), we may draw the conclusion that the model is relatively insensitive to varying gamma values. Concluding, g does not need to be adjusted to fit field data.

The current bed shear stress is related to the horizontal velocity scaled by the drag coefficient. The drag coefficient is proportional to the Manning number squared. The tests indicate the model predictions vary with variations of the Manning number but are not overly sensitive. The model was sensitive to small changes in wave angle when waves were near shore normal and the bathymetry was complex. Significant changes in skill took place with small adjustments to the wave angle. As it is difficult to accurately measure wave angle this is an important circumstance in the model assessment.

The asymmetry coefficient primarily responsible for moving sediment onshore due to cross-shore wave velocity asymmetry strongly affects model sediment transport.

Qualitatively there is reasonably good agreement between measured and predicted sediment distribution over the 2-D minigrid area when a_w = .25 or a_w = .3. The rip channel was modeled in roughly the same location and with a clearly developed channel. Further study is required to calibrate the model.

Man made objects affect the wave, flow, and sediment dynamics. The model does not resolve sub grid objects like the pier pilings. Man made objects can produce turbulent eddies which are on a time and special scale smaller than the model can resolve. A possibility would be to explore is the idea of parameterizing the bottom stress of the model to take into account the turbulence by a man made object.

LIST OF REFERENCES

Arcilla A.S., J.A. Roelvink, B.A. O'Connor, A. Reniers, and J.A. Jimenez, "The Delta flume'93 experiment," *Proceedings Coastal Dynamics '94*, 488-502, Am. Soc. of Civ. Eng., 1994.

Battjes, J.A. and J.P.F.M Janssen, "Energy Loss and Set-Up Due to Breaking Waves," *Proceedings of the 16th International Conf. on Coastal Engineering*, 569, Am. Soc. of Civ. Eng., 1978.

Fredsoe, J., "Turbulent Boundary Layer in Wave-Current Motion," *Journal Hydraul. Eng*., ASCE, 110, 1,103-1,120, 1984.

Fredsoe, J. and R. Deigaard, "Mechanics of Coastal Sediment Transport," World Scientific Publishing, Singapore, 1992.

Galappatti, R., "A Depth Integrated Model for Suspended Transport," *Delft University report no. 83-7*, Delft University of Technology, Dept of Civil Eng., The Netherlands, 1983.

Gallagher, E.L., S. Elgar, and R.T. Guza, "Observations of Sand Bar Evolution on a Natural Beach," *J. Geophys. Res.*, 103(C2), 3203-3215, 1998.

Holthuijsen, L.H., N. Booij, and T.H.C. Herbers, "A Prediction Model for Stationary, Short-Crested Waves in Shallow Water with Ambient Currents," *Coastal Engineering*, 13, 23-54, 1989.

Nairn, R.B., J.A. Roelvink, and H.N. Southgate, "Transition Zone Width and Implications for Modeling Surfzone Hydrodynamics," *Proceedings of the 22nd International Conf. on Coastal Engineering, 68-81*, Am. Soc. of Civ. Eng., 1990.

Phillips O.M., "The Dynamics of the Upper Ocean," Cambridge University Press, Cambridge, Great Britain, 1977.

Reniers A.J.H.M., G. Symonds, E.B. Thornton, "Modelling of Rip Currents During Rdex," *Proceedings Coastal Dynamics '01*, 493-499, Am. Soc. of Civ. Eng., 2001.

Reniers, A.J.H.M., J.A. Roelvink and E.B. Thornton, "Morphodynamic Modeling of an Embayed Beach Under Wave Group Forcing," submitted to *J. Geophys. Res*., 2002.

Reniers, A.J.H.M, J. MacMahan, E.B. Thornton, and T. Stanton, "Infragravity Motions on a Complex Beach, Part II: Modeling," (in preparation 2002)

Roelvink, J.A., and M.J.F. Stive, "Bar-Generating Cross-Shore Flow Mechanisms on a Beach," *J. Geophys. Res*., 94(C4), 4785-4800, 1989.

Roelvink, J.A., "Dissipation in Random Wave Groups Incident on a Beach," *Coastal Engineering*, 19, 127-150, 1993.

Roelvink, J.A., and I. Broker, "Cross-Shore Profile Models," *Coastal Engineering*, 21, 163-191, 1993.

Ruessink, B.G., "Infragravity Waves in a Dissipative Multiple Bar System," *Ph. D. Thesis*, University of Utrecht, 245 pp, 1998.

Soulsby, R.L., "Dynamics of Marine Sands," Thomas Telford Publishing, London, England, p 87-95, 1997.

Soulsby, R.L., L. Hamm, G. Klopman, D. Myrhaug, R.R. Simons, and G.P. Thomas, "Wave-Current Interaction Within and Outside the Bottom Boundary Layer," *Coastal Engineering*, 21, 41-69, 1993.

Stokes, G.G., "On the Theory of Oscillatory Waves," *Trans. Camb. Phil. Soc.*, 8, 441-455, 1847.

Thornton, E.B. and R.T. Guza, "Surf Zone Longshore Currents and Random Waves: Field Data and Models," *J. Geophys. Res.*, 16(7), 1,165-1,178, 1986.

Thornton, E.B., R.T. Humiston, and W. Birkemeier, "Bar/Trough Generation on a Natural Beach," *J. Geophys. Res.*, 101(C5), 12,097-12,110, 1996.

Thornton, E.B., and C.S. Kim, "Longshore Current and Wave Height Modulation at Tidal Frequency Inside the Surf Zone," *J. Geophys. Res.*, 98(C9), 16,509-16,519, 1993.

van Rijn, L.C., "Principles of Sediment Transport in Rivers, Estuaries, and Coastal Seas," Aqua Publications, Amsterdam, Netherlands, 1993.

INITIAL DISTRIBUTION LIST

1. Defense Technical Information Center
   Ft. Belvoir, Virginia

2. Dudley Knox Library
   Naval Postgraduate School
   Monterey, California

3. Dr. Ed Thornton, Department of Oceanography
   Naval Postgraduate School
   Monterey, California

4. Dr. Ad Reniers, Department of Oceanography
   Naval Postgraduate School
   Monterey, California